



Materials modelling and process simulation of the pultrusion of curved parts

G. Struzziero^{a,*}, G.M. Maistros^b, J. Hartley^c, A.A. Skordos^a

^a School of Aerospace, Transport and Manufacturing, Cranfield University, Bedford MK43 0AL, UK

^b ADVISE-DETA Ltd, Chios 82100, Greece

^c Exel Composites, Runcorn WA7 3DU, UK

ARTICLE INFO

Keywords:

- A. Polymer-matrix composites (PMCs)
- B. Thermomechanical
- C. Process modelling
- E. Cure

ABSTRACT

The present paper addresses the simulation of a concept for the manufacturing of aerospace quality carbon/epoxy composite curved parts using pultrusion. In this approach, the part is first partially cured in a pre-former followed by final curing in a curved post-former. An aerospace epoxy resin system has been fully characterised and the corresponding constitutive material models, incorporating dependence on both temperature and degree of cure, developed. A 3D Finite Element model of the process, to manufacture a T-stiffener, involving impregnation, curing and forming of the curvature was developed and implemented. The simulation results show that a degree of cure of around 62% -close to the gelation point of the resin system considered - at the exit of the pre-former stage is appropriate for the success of the subsequent stage. In the post-former the cure is completed reaching a final degree of cure of about 87%. The stresses generated in post-forming reach a maximum of 54 MPa in compression in the transverse direction and of 200 MPa in tension in the fibre direction showing that the process is feasible without inducing defects linked to micro buckling or rupture.

1. Introduction

Pultrusion is a continuous process carried out through impregnation of dry or pre-impregnated reinforcement guided into a die to attain the desired cross sectional lay-up and profile followed by heating to achieve curing of the material. By its nature, pultrusion produces straight constant profile parts, with the process being highly cost efficient in applications requiring large length composite profiles of constant cross section. The quality of the final product is governed by both flow effects, controlling the generation of voids and dry spots, and thermal/curing effects, controlling temperature overshoots, which arise as a result of significant heat release by the curing reaction combined with the limited heat dissipation through the thickness of the composite material, residual stress levels and final material state.

In the case of dry reinforcement, pultrusion impregnation phenomena can be simulated by solution of Darcy's law in a moving frame of reference. Two-dimensional solutions of the flow problem for simple tapered geometries have been successfully developed to predict the pressure distribution, flow front profile [1–4] and pultrusion pulling force [5–7]. Existing simulation tools for liquid composite moulding processes can be modified and adapted to the solution of the flow stage

of a pultrusion process [8]. Simulation of the curing stage and of the relevant thermochemical effects has been developed allowing the prediction of the temperature and degree of cure distribution [9–15]. Solution of the thermochemical model has been implemented in an optimisation framework to determine process designs that minimise degree of through thickness cure gradients [16–19] and process time [20,21]. The coupled thermomechanical problem has also been addressed to allow prediction of residual stress development during the pultrusion process [22,23]. Curved parts have been manufactured using pultrusion by inducing a controlled curvature using a robot arm and UV curing [24,25]. Moreover, concepts for thermoplastic matrix composites pultrusion of curved geometries [26] as well as single stage thermosetting matrix composite curved pultrusion [27] have been put forward. These efforts show the feasibility of using pultrusion to manufacture curved parts.

The current work combines the concept of curved pultrusion with a conventional heated die process in a two stage approach for composite components using thermoset matrix and through the development of detailed material models and the associated thermomechanical-chemical FE simulation investigates the process evolution and outcome in terms of degree of cure and process stress due to thermal

* Corresponding author.

E-mail address: Giacomo.struzziero@empa.ch (G. Struzziero).

expansion/contraction, cure shrinkage, bending and contact with the die. The work presented here focuses on 3D flow and thermomechanical simulation of the pultrusion of curved parts. The paper introduces the manufacturing concept for the production of aerospace quality parts, based on implementation of an additional stage (i.e. post-former) to standard pultrusion. A material characterisation campaign for a typical pultrusion epoxy resin system including rheological, chemical, thermal, mechanical and thermomechanical properties has been undertaken. Incorporation of the corresponding material models into FE numerical analysis allows prediction of the viscosity, degree of cure and thermal gradients at the end of the impregnation and pre-former stage and degree of cure, thermal gradients and residual stresses at the end of the post-former stage. The results of the simulation are set against the outcomes of process trials to assess the quality of the simulation. Furthermore, the simulation predictions are used to analyse the feasibility of manufacturing curved aerospace quality parts using the proposed concept.

2. Pultrusion process for curved parts manufacturing

The pultrusion concept presented here aims to achieve production of curved parts on the pultrusion line complying with the requirements of the aerospace industry. A schematic of the concept is illustrated in Fig. 1. The line can be divided into two stages. Stage one corresponds to conventional pultrusion manufacturing. The raw dry material is pulled into the desired configuration before entering the die. An injection system is used at the entry of the die to facilitate impregnation of the reinforcement which is compacted in the final profile shape. This step could also involve use of a resin bath as an alternative without application of an injection pressure. Subsequently, the impregnated profile enters the pre-former die where a partially cured profile is produced. In the implementation of this study, curing is carried out by two 25 cm long heaters incorporated on the die. The gap between the two heaters is 7 cm. A schematic representation of the pre-former is reported in Fig. 2a. After exiting the pre-former, the part is partially cured and stage one is complete. Stage two takes the partially cured part and completes the curing through a curved post-former die. In the post-former the partially cured part is heated above its glass transition temperature to allow bending and forming combined with final curing. The die in the implementation considered here includes two heaters covering 17° of the arc placed at a distance of 11° between them and 6° from the die entry and exit as shown in Fig. 2b.

3. Materials and methodology

This section introduces the governing equations for pultrusion simulation followed by a description of the materials used and the geometry of the part manufactured. This is followed by a presentation of the constitutive models for the cure kinetics, glass transition temperature evolution and thermal properties. The experimental procedures used to measure permeability and viscosity are also described as well as the experimental methodology used to characterise modulus, coefficient

of thermal expansion and chemical shrinkage of the resin.

3.1. Pultrusion modelling principles

The solution of stage one of the process involves consideration of flow through porous media as well as heat transfer due to conduction and material advection accompanied by heat generation for the curing reaction. The flow through porous media problem is addressed by combining the continuity equation with Darcy's law as follows:

$$\nabla \cdot \left(\frac{\mathbf{S}}{\eta} \nabla p \right) = 0 \quad (1)$$

where \mathbf{S} is the permeability tensor, η the viscosity and p the pressure. The solution of this equation involves several constitutive material models including the dependence of permeability on local volume fibre fraction and the evolution of resin viscosity.

The heat transfer model of stage one takes into account heat conduction, exothermic contributions from curing and heat advection as follows:

$$\rho_c c_p \left(\frac{\partial T}{\partial t} + \vec{u} \cdot \nabla T \right) = \nabla \cdot (\mathbf{K} \nabla T) + \rho_r v_r H_{tot} \frac{d\alpha}{dt} \quad (2)$$

where \vec{u} is the velocity of the resin flow for stage one and translational velocity of pultrusion for stage two, ρ_c , c_p are the density and specific heat of the composite, \mathbf{K} is the thermal conductivity tensor, ρ_r the resin density, H_{tot} the total heat flow and α the degree of cure.

The solution for stage two involves a coupled thermomechanical model which combines Eq. (2) with a momentum balance, which for the quasistatic case and assuming no flow in this stage of the process becomes:

$$\nabla \cdot \boldsymbol{\sigma} = 0 \quad (3)$$

where $\boldsymbol{\sigma}$ the stress tensor. This is accompanied by a Cure Hardening Instantaneously Linear Elastic (CHILE) material model including dependence of properties on temperature and degree of cure. The incremental form of the CHILE model is:

$$\Delta \boldsymbol{\sigma} = \mathbf{C}(\alpha, T) (\Delta \boldsymbol{\varepsilon}_{tot} - \boldsymbol{\alpha}_{TH}(\alpha, T) \Delta T - \boldsymbol{\gamma}_{CH}(\alpha, T) \Delta \alpha) \quad (4)$$

where \mathbf{C} denotes the stiffness matrix, $\boldsymbol{\sigma}$ the stress tensor, $\boldsymbol{\varepsilon}_{tot}$ the total strain tensor, $\boldsymbol{\alpha}_{TH}$ the thermal expansion coefficient matrix and $\boldsymbol{\gamma}_{CH}$ the chemical coefficient matrix of the composite material.

3.2. Materials and geometry

The materials of this study are HTA40 carbon fibres [28] and an epoxy system formulated using Huntsman® XU3508 prepolymer, Huntsman® XB3473 hardener [29] and 4% PAT®-656/B3R release agent [30]. The part manufactured is a curved T cross section stiffener. The part comprises a flange and a web, which form a noodle at the centre of the cross section. Fig. 2c illustrates half of the cross section of the T-

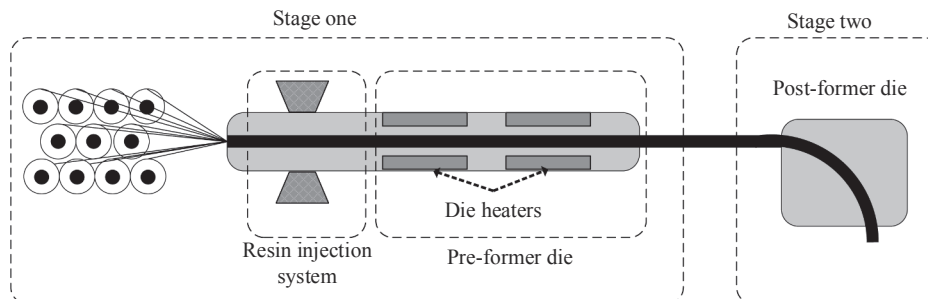


Fig. 1. Pultrusion schematic.

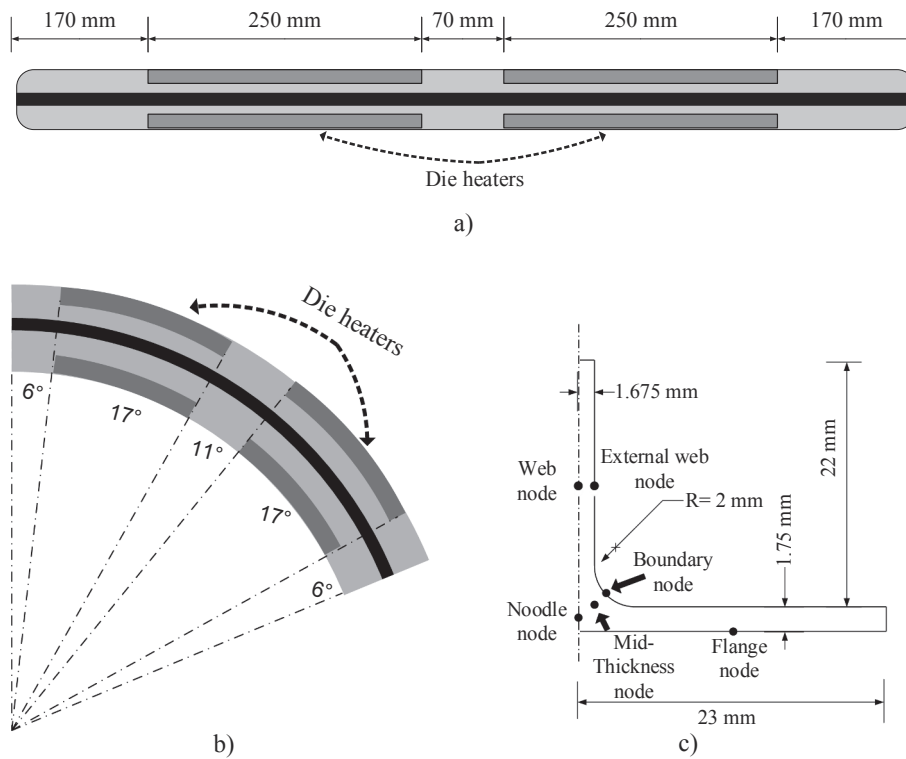


Fig. 2. a) Pre-former b) Post-former c) Half of the cross section of the T-stiffener showing representative nodes.

stiffener. The thickness of the web is 3.35 mm and of the flange 1.75 mm. The width of the flange is 46 mm and the height of the web 22 mm. The cross section of the noodle forms a three-sided concave shape with a fillet radius of 2 mm. The post-former induces an inner curvature of 1.064 m^{-1} (radius of 0.94 m) over a 57° arc. The stiffener is made of two reinforcement forms: UD carbon tows (HTA, 12 K, TohoTenax®) [28] with a linear weight of 0.8 g/m and a triaxial carbon braid with tows in the $\pm 45^\circ$ and 0° directions with an areal weight of 440 g/m^2 and a width of 46 mm. The web comprises 4 layers of braid and 3 of UD made of 18 tows each. The flange is made of 3 layers of braid and 2 layers of UD material made of 10 tows in the continuous region and 5 tows on each side in the region divided by the noodle. The noodle consists of UD tape oriented in the pultrusion direction. The fibre volume fraction calculated considering the areal weight of both reinforcements and the number of layers used in the different regions assuming an *iso-stress* condition in the thickness direction is 65% in the web, 56% in the flange and 58% in the noodle. Table 1 summarises the overall lay up for the different regions of the component.

Table 1
Laminate details of the T-stiffener.

Region	Orientation wrt pultrusion direction	Thickness (mm)
Web	$[0 + 45-45]_s$	0.3972
	0	0.5872
	$[0 + 45-45]_s$	0.3972
	0	0.5872
	$[0 + 45-45]_s$	0.3972
	0	0.5872
Flange	$[0 + 45-45]_s$	0.462
	0	0.182
	$[0 + 45-45]_s$	0.462
	0	0.182
	$[0 + 45-45]_s$	0.462
Noodle	0	Entire cross section

3.3. Cure kinetics and glass transition temperature

The chemical and thermal properties of the resin under study have

Table 2

Parameter values for the cure kinetics and thermal material models for the XU3508 / XB3473 epoxy system [27].

Cure kinetics	
$A(\text{s}^{-1})$	759
$E(\text{J}\cdot\text{mol}^{-1})$	47,850
n	1.25
C	80
α_c	0.17
$\alpha_T(\text{K}^{-1})$	0.00631
$H_{tot}(\text{Jg}^{-1})$	250
Di Benedetto	
$T_{g0} \text{ }^\circ\text{C}$	-20
$T_{g\infty} \text{ }^\circ\text{C}$	160
λ	0.371
Specific heat	
$C_{rub}(\text{Jg}^{-1}\text{ }^\circ\text{C}^{-1})$	1.36
$C_{rubT}(\text{Jg}^{-1}\text{ }^\circ\text{C}^{-2})$	1.36×10^{-3}
$C_{rub\alpha}(\text{Jg}^{-1}\text{ }^\circ\text{C}^{-1})$	0.080
$C_{glass}(\text{Jg}^{-1}\text{ }^\circ\text{C}^{-1})$	0.305
$C_{glassT}(\text{Jg}^{-1}\text{ }^\circ\text{C}^{-2})$	8.97×10^{-3}
$C_w(\text{ }^\circ\text{C}^{-1})$	0.935
$\sigma^c C$	74.0
σ_T	-0.714
Thermal conductivity	
$\theta(\text{W m}^{-1} \text{ K}^{-1})$	0.44
$\beta(\text{W}^{-1} \text{ m K})$	-12.1
$\gamma(\text{m W}^{-1})$	0.061

been characterised and reported in [31]. Table 2 reports the corresponding parameters for the constitutive models. The cure kinetics model utilised involves a diffusion limitation term [32]. The reaction rate depends on both temperature and degree of cure and can be expressed as follows:

$$\frac{d\alpha}{dt} = \frac{A \exp\left(\frac{-E}{RT}\right)}{1 + \exp(C(\alpha - \alpha_c - \alpha_T T))} (1 - \alpha)^n \quad (7)$$

where n the reaction order, T the temperature in Kelvin, E the activation energy, A the pre-exponential factor, R the universal gas constant, C a constant controlling the breadth of the transition from chemical to diffusion control of the kinetics, α_c , α_T coefficients controlling the transition degree of cure depending on temperature and n the reaction order.

The glass transition temperature model of the resin system adopted follows the dependence described by the Di Benedetto equation [33] as follows:

$$T_g = T_{g0} + \frac{(T_{g\infty} - T_{g0})\lambda\alpha}{1 - (1 - \lambda)\alpha} \quad (8)$$

where T_{g0} denotes the glass transition temperature of the uncured material, $T_{g\infty}$ the glass transition temperature of the fully cured material and λ is a fitting constant which control the convexity of the non-linear dependence.

3.4. Thermal properties

The specific heat constitutive model of the composite accounts for the contribution from both the resin system and carbon fibres through the rule of mixtures:

$$c_p = w_f c_{pf} + (1 - w_f) c_{pr} \quad (9)$$

where w_f is the fibre weight fraction, c_{pf} the specific heat capacity of the fibres and c_{pr} the specific heat capacity of the resin. The specific heat of carbon fibres follows a linear dependence on temperature [34]:

$$c_{pf} = A_{fcp} T + B_{fcp} \quad (10)$$

here A_{fcp} is the slope of the linear dependence and B_{fcp} the intercept. The specific heat capacity of the resin system depends on both temperature and degree of cure and is described as follows [31]:

$$c_{pr} = C_{rub} + C_{rub\alpha}\alpha + C_{rubT}T + \frac{(C_{glass} + C_{glassT}T - C_{rub} - C_{rub\alpha}\alpha - C_{rubT}T)}{1 + \exp(C_w(T - T_g - \sigma - \sigma_T T))} \quad (11)$$

where C_{rub} , $C_{rub\alpha}$, C_{rubT} control the specific heat capacity dependence on temperature and degree of cure in the rubber state, whilst C_{glass} , C_{glassT} control the value in the glass state. The behaviour around the glass transition is controlled by C_w which governs the breadth of the transition and σ , σ_T which define the temperature shift.

The thermal conductivity of the composite is the result of the contribution from both resin system and carbon fibres and it is computed as follows for the longitudinal and transverse directions respectively [34,35]:

$$K_{11} = v_f K_{1f} + (1 - v_f) K_r \quad (12)$$

$$K_{22} = K_{33}$$

$$= v_f K_r \left(\frac{K_{1f}}{K_r} - 1 \right) + K_r \left(\frac{1}{2} - \frac{K_{1f}}{2K_r} \right) + K_r \left(\frac{K_{1f}}{K_r} - 1 \right) \sqrt{v_f^2 - v_f + \frac{\left(\frac{K_{1f}}{K_r} + 1 \right)^2}{\left(\frac{2K_{1f}}{K_r} - 2 \right)^2}} \quad (13)$$

where K_{1f} and K_{2f} are the thermal conductivity of fibres in the axial and transverse direction, K_r is the thermal conductivity of the resin and v_f the volume fibre fraction. The thermal conductivity of carbon fibres in the axial direction (K_{1f}) is a linear function of temperature, whilst in the transverse direction (K_{2f}) it can be considered constant [34,36]:

$$K_{1f} = A_{1f} T + B_{1f} \quad (14)$$

$$K_{2f} = B_{2f} \quad (15)$$

The thermal conductivity of the resin depends on both temperature and degree of cure and is governed by the following equation [31]:

$$K = \frac{1 + \theta\alpha}{\beta + \gamma T} \quad (16)$$

where θ is a fitting parameter controlling the linear dependence on degree of cure, β is the contribution of structure scattering and of vacant-site scattering to thermal resistance; γ is a fitting parameter governing the dependence on absolute temperature.

3.5. Rheological and hydraulic properties

The rheology of the resin has been investigated through five isothermal rheometry tests at 80 °C, 90 °C, 100 °C, 110 °C and 120 °C. The shear rate applied was 10 s⁻¹. A TA Instruments AR2000ex rheometer was used with a cone and plate configuration. The 2° cone had a diameter of 40 mm with a truncation depth of 54 μm.

Saturated permeability tests were performed on the triaxial braid along both in-plane directions and the UD tows. The mould used for the tests had a cavity of 100 mm width and 400 mm length. An O-ring with diameter of 2 mm was used around the male part of the upper part of the mould to ensure sealing. The fabric size inserted into the mould had dimensions of 100 mm × 300 mm, as there was a free space near the inlet and the outlet ports. The thickness of the cavity was 4 mm. For measurement of the braid permeability in the longitudinal and transverse directions, eight layers of braid were cut and placed in the mould taking care to avoid overlaps or gaps at the border of the braid sections. For the measurement of the permeability of the UD reinforcement sets of tows of length 300 mm were cut and arranged to fill the width of the mould. In both cases the reinforcement was secured by clamping 5 mm of its ends to the lower plate of the mould and shifting was not observed during the permeability tests. As soon as the mould was closed, vacuum was applied at the vent and the tube from the inlet port was immersed into a silicone oil container. The pressure difference between the inlet and outlet port was 90 kPa. Permeability tests were repeated three times for each case. A PDMS silicone oil of medium nominal viscosity by Clearco was used for the tests. The silicone oil viscosity was 0.194 Pas. The reinforcement areal density was used to calculate the fibre volume fraction.

3.6. Mechanical and thermomechanical properties

The mechanical properties of the curing composite material were computed through implementing micromechanical relations and using the properties of resin and fibre. The Chamis formulation was implemented to compute the elastic properties of the composite. The longitudinal modulus of the composite material in the fibre (E_l), transverse (E_t), shear (G_{12}) directions and the in plane Poisson's ratio (ν_{12}) are

expressed as follows:

$$E_l = \nu_f E_{lf} + (1 - \nu_f) E_r \quad (17)$$

$$E_t = \frac{E_r}{1 - \sqrt{\nu_f} \left(1 - \frac{E_r}{E_{lf}}\right)} \quad (18)$$

$$G_{12} = \frac{G_r}{1 - \sqrt{\nu_f} \left(1 - \frac{G_r}{G_{12f}}\right)} \quad (19)$$

$$\nu_{12} = \nu_f \nu_{12f} + (1 - \nu_f) \nu_r \quad (20)$$

where E_r , G_r and ν_r are the Young's modulus, shear modulus and Poisson's ratio of the resin and E_{lf} , E_{tf} , G_{12f} and ν_{12f} are the longitudinal, transverse and shear modulus and Poisson's ratio of the fibre [37,38]. The modulus of the resin system has been evaluated by manufacturing four partially cured plates at 67%, 79%, 85% and fully cured and testing using a Q800 TA Instruments Dynamic Mechanical Analyser (DMA). A single cantilever beam was used with heating applied at a rate of 3 °C/min.

The longitudinal and transverse coefficient of thermal expansion expression can be expressed as follows applying micromechanics laws [39]:

$$a_l = \frac{(1 - \nu_f) E_r a_r + \nu_f E_{lf} a_{lf}}{(1 - \nu_f) E_r + \nu_f E_{lf}} \quad (21)$$

$$a_t = (1 - \nu_f) a_r + \nu_f a_{tf} + (1 - \nu_f) a_r \nu_r + \nu_{12f} a_{lf} \nu_f - \nu_{12} a_l \quad (22)$$

where a_l and a_t are the coefficients of thermal expansion of the composite in the fibre and transverse direction respectively, a_r is the coefficient of thermal expansion of the resin and a_{lf} , a_{tf} the thermal expansion coefficient of the carbon fibre in the axial and transverse direction respectively. The fibre coefficients are temperature dependent following a polynomial law as follows [40]. Values referring to HTA5131 carbon fibres have been used in the present study.

$$a_{lf} = \sum_{i=0,4} A_{a_{lf}}^i T^i \quad (23)$$

$$a_{tf} = \sum_{i=0,3} A_{a_{tf}}^i T^i \quad (24)$$

Specimens from the partially cured plates have been used to measure the coefficient of thermal expansion (CTE) using a 2940 TA Instrument Thermal Mechanical Analyser (TMA). The dimensions of the TMA specimens were 3 mm × 3 mm × 3 mm. A ramp rate of 3 °C/min was utilised.

The anisotropic shrinkage of the composite can be modelled as follows:

$$\gamma_l = \frac{(1 - \nu_f) E_r \gamma_r}{(1 - \nu_f) E_r + \nu_f E_{lf}} \quad (25)$$

$$\gamma_t = (1 - \nu_f) \gamma_r + (1 - \nu_f) \gamma_r \nu_r - \nu_{12} \gamma_l \quad (26)$$

$$\gamma_r = \gamma_v \alpha \quad (27)$$

where γ_l is the shrinkage in fibre direction, γ_t the shrinkage in the transverse direction and γ_r is the isotropic shrinkage of the resin that can be assumed a linear function of degree of cure and γ_v is volumetric shrinkage.

The shrinkage of the curing resin has been measured in isothermal tests using an in-house setup based on the gravimetric method reported in [41]. Fig. 3 shows the experimental set-up. The measurement exploits the effect of buoyancy forces. Silicone oil is placed in a cylindrical

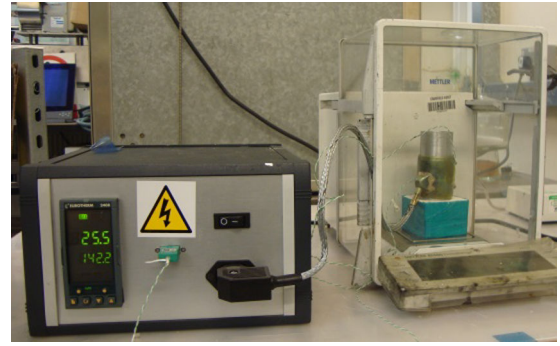


Fig. 3. Shrinkage measurement set-up. (For interpretation of the references to colour in this figure legend, the reader is referred to the web version of this article.)

aluminium container and heated up by means of a heating element and controlled using a 2408 Eurotherm controller. The aluminium container is placed on an insulating plate on a scale. Silicone bags have been manufactured mixing silicone rubber T20 and T6 catalyst. The mixture was spread on PTFE rods 7 mm in diameter and let to cure at room temperature for 24 h, followed by a 3 h post cure at 100 °C. In order to avoid changes in volume due to absorption of silicone oil, the silicone bags were conditioned by immersing in silicone oil at room temperature for 5 days and at 150 °C for 2 days. No change in weight of the bags has been recorded at the end of the conditioning cycle. To carry out the shrinkage measurement resin is poured into the silicone bags and squeezed in order to achieve a quasi-spherical shape; the bag is then clamped using a clip. The clip is hung to a support using a thread and the bag is immersed into the silicone oil. The resin is subsequently cured inside the silicone bag. The whole system without the silicone bag has a weight which is recorded by the scale. Once the silicone bag containing the resin is immersed, a reaction force to buoyancy comes into play. The scale detects an increase in weight equal to:

$$F_A = (V_{bag} + V_{resin}) \rho_{liquid} g \quad (28)$$

where V_{bag} , V_{resin} are the volumes of the silicone bag and resin respectively, ρ_{liquid} is the density of the silicone oil and g the acceleration of gravity. As a result of shrinkage V_{resin} decreases causing a reduction of the weight recorded. Two isothermal tests have been carried out at 110 °C and 130 °C.

4. Simulation

The following sections provide the details for the numerical analysis of stage one and stage two respectively.

4.1. Stage one simulation

The coupled thermochemical and Darcy flow problem described by Eqs. (1) and (2) to simulate stage one has been modelled using the Control Volume/Finite Element solver PAMRTM® [42]. Braid layers were modelled using an equivalent lay up of [0 +45 -45]_s. The model utilises three-dimensional hexahedral elements split in two triangular prisms and comprises 13,296 nodes and 33,699 elements. The mesh used is shown in Fig. 4. Only half of the T-profile has been modelled due to symmetry. Pressure and fixed temperature boundary conditions were applied along the length of the profile through user defined tables. The state of the boundary conditions is time dependent in order to activate them upon entry in the die (temperature) and at the injection point (pressure) and deactivate them at the exit of the die for temperature and once passed the injection point for pressure [8]. Fig. 5 illustrates a schematic of the operation of the pressure moving boundary condition. High pressure injection is represented by a prescribed pressure boundary

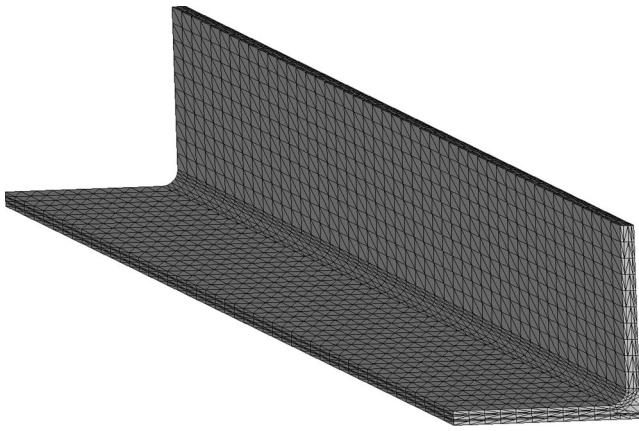


Fig. 4. Finite element mesh of the T stiffener for stage one of the curved pultrusion process.

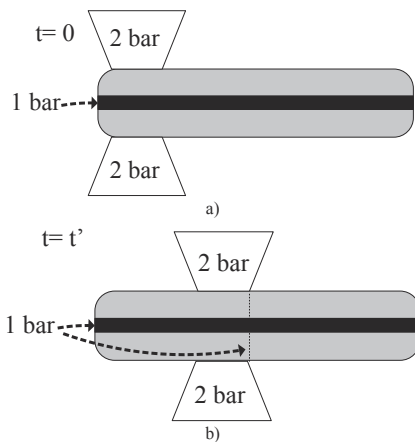


Fig. 5. Moving pressure boundary conditions at a) $t = 0$ and; b) $t = t'$.

condition applied to all nodal points that come within the injection region during the process. In this condition, the pressure is equal to the injection pressure when a node is within the injection port region, whereas the condition is deactivated when the node is outside this region. Similarly, the pressure at all non-surface nodes is equal to atmospheric when they are located at the entry point and at the end of pultrusion, and the corresponding boundary condition is deactivated at all other locations. The current development allows simulation of a pultrusion process in which impregnation occurs in an injection chamber. In this case, the free boundary capabilities of the code are used to determine the backflow of the resin outside the die and the extent of wetting in the reinforcement coming through the entry point. The viscosity, cure kinetics and thermal properties sub-models have been implemented through user-defined tables.

In the stage one pultrusion simulation the temperature of the heaters was set to 160 °C and the pulling speed at 5 cm/min. The heater temperature is applied directly to the nodes of the outer surface of the pultrusion material. The pressure of the injection used was 2 bar, whilst the atmospheric pressure was considered equal to 1 bar.

4.2. Stage two simulation

The coupled thermomechanical-chemical phenomena taking place during stage two of the process, expressed by Eqs. (2)–(4), have been modelled using the finite element solver Marc® [43]. Three-dimensional 20-nodes composite brick element (Marc® element type 150) were utilised [44]. The model comprises 78,321 nodes and 13,940 elements.

In order to deform the part into the desired final curved shape, the part itself has been modelled as a deformable contact body and the die as a rigid contact body. A large strain formulation is used in the finite element solution. The part is assumed to be stress free in its bent configuration upon entry in the post-former. This reflects the fact that the material is heated well over its instantaneous glass transition temperature reached in the first stage and therefore its modulus is very low (in the order of MPa), which allows stress relaxation and prevents stress build up. A sliding condition between the part and die has been applied. In the model the part is represented by 44,698 nodes and 9240 elements and the die by 33,623 nodes and 4700 elements. The mesh used is illustrated in Fig. 6. The initial degree of cure condition applied corresponds to a value equal to the degree of cure at the exit of stage one. Braid layers are modelled using an equivalent lay up of $[0 +45 -45]_s$. Time dependent prescribed displacement boundary conditions have been implemented using the FORCDT user subroutine [45]. Thermal boundary conditions inside and outside the post-former die have been applied by subroutine UFILM. A surface heat transfer coefficient of 50 $\text{W}/\text{m}^2\text{K}$ [46,47] has been used between the inlet and first heater, the two heaters, and second heater and outlet, whilst at the heaters location the convection coefficient has a high value ($1000 \text{ W}/\text{m}^2\text{K}$) so that the nominal heater temperature is applied to the part nodes under the heater. The coefficient outside the die is $13.6 \text{ W}/\text{m}^2\text{K}$ [48]. The pulling speed was 5 cm/min and the two heaters in the post-former were set at 170 °C.

The sub-models for cure kinetics, glass transition specific heat capacity and thermal conductivity were implemented using the UCURE, USPCHT and ANKOND user subroutines following the models reported for stage one. The sub-models for mechanical moduli, Poisson ratio, coefficient of thermal expansion and shrinkage were implemented using the HOOKLW, ANEXP and USHRINKAGE user subroutines. A flow chart representing the interactions between the three different models have been added as in Fig. 7.

5. Results and discussion

5.1. Hydraulic and rheological material properties

The viscosity model implemented to fit the experimental data uses temperature and degree of cure as state variable implying the coupling with cure kinetics [49]. The equation describing the relationship is:

$$\eta = \eta_0 \exp\left(\frac{U}{RT} + K_1 \alpha + K_3 \alpha^3\right) \quad (29)$$

where U , K_1 , K_3 are fitting parameters, η_0 the initial viscosity at very high temperature and T is temperature expressed in Kelvin. The resulting fitting is depicted in Fig. 8. The average relative error of the

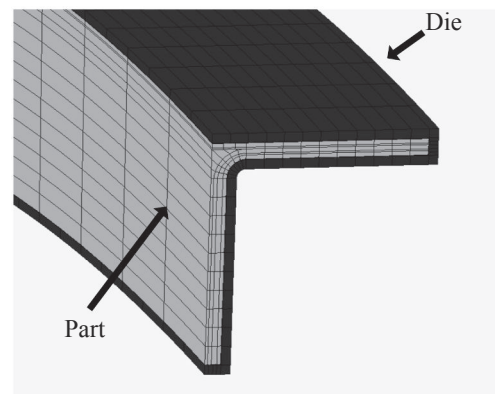


Fig. 6. Finite element mesh of the T stiffener for stage two of the curved pultrusion process.

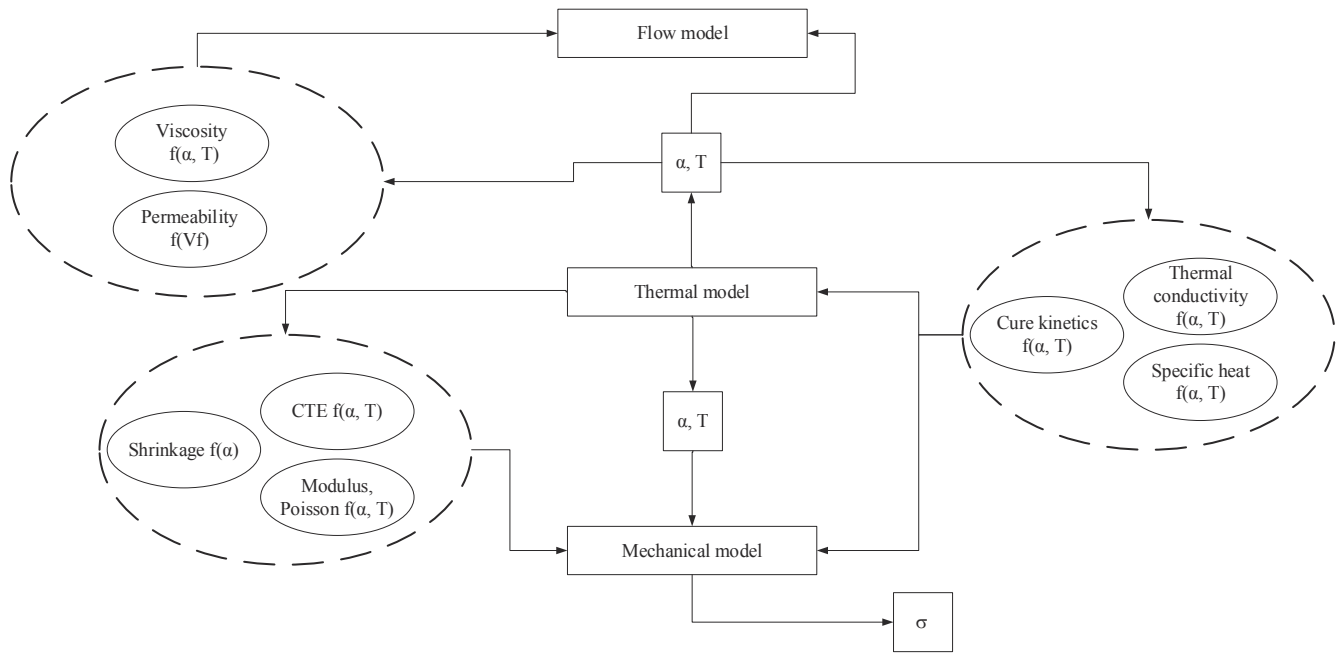


Fig. 7. Interdependencies of models and constitutive material properties in the simulation of two stage pultrusion process.

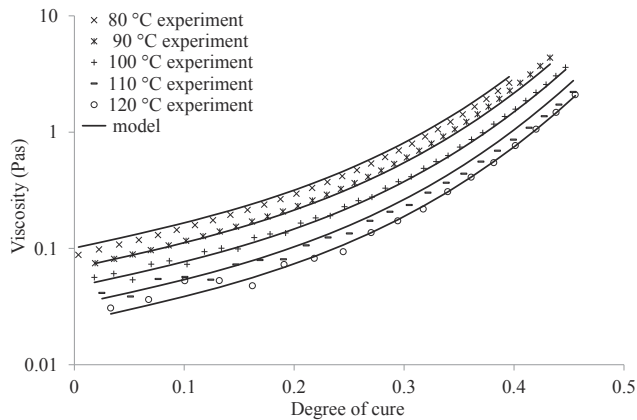


Fig. 8. Fitting of rheology experimental data for the XU3508 / XB3473 epoxy system.

fitting is 8%. Table 3 reports the fitting parameter for the viscosity model and the results of the permeability tests. The permeability values used in the model corresponding to the volume fibre fraction of the part at different locations have been calculated using the Kozeny-Carman equation and the Gebart model from the measured values. The Kozeny-Carman equation has been considered appropriate for biaxial braid [50,51], whereas the Gebart model [52] provides an improved solution that is easily applicable to UD materials. An intermediate shape between hexagonal and square has been considered appropriate. The values obtained are reported in Table 4 together with the measured values. The value of permeability in the through thickness direction of the reinforcement has been assumed to be equal to the permeability in their transverse direction.

5.2. Mechanical and thermomechanical material properties

The modulus of the resin has been modelled using the following expression:

Table 3
Parameter values for the viscosity, modulus, CTE and shrinkage constitutive models for the XU3508 / XB3473 epoxy system.

Parameters	Viscosity Values	Units
U	42,120	$J mol^{-1}$
K_1	4.75	
K_3	24.4	
η_0	5.94×10^{-8}	Pas
Modulus		
E_{rub}	0.025	GPa
E_{glass}	2.9	GPa
E_{glassT}	-0.011	$GPa \text{ } ^\circ C^{-1}$
C_m	0.33	$^\circ C^{-1}$
σ_m	5	$^\circ C$
CTE		
a_{rub}	0.00039	$^\circ C^{-1}$
$a_{rub\alpha}$	-0.00021	$^\circ C^{-1}$
a_{glass}	0.000075	$^\circ C^{-1}$
C_{CTE}	0.15	$^\circ C^{-1}$
σ_{CTE}	1	$^\circ C$
Shrinkage		
γ_v	0.0833	

$$E_r = E_{rub} + \frac{(E_{glass} + E_{glassT}T - E_{rub})}{1 + \exp(C_m(T - T_g - \sigma_m))} \quad (30)$$

where E_{glass} is the modulus of the resin in the glass state, E_{rub} the modulus in the rubber state. The linear sensitivity of modulus on temperature in the glass state is expressed by E_{glassT} , whilst C_m governs the breadth of the transition and σ_m the temperature shift. Fig. 9 reports the fitting of the model to the experimental data, corresponding to an average relative error of 8%. The CTE of the resin follows a step transition around the glass transition represented by the following expression:

Table 4
Permeability values for the braid and UD material.

	Fibre volume fraction	UD		Braid	
		Longitudinal permeability (m^2)	Transverse permeability (m^2)	Longitudinal permeability (m^2)	Transverse permeability (m^2)
Experimental	58%			6.46×10^{-11}	6.66×10^{-11}
	50%	3.30×10^{-10}			
Computed	56%	1.62×10^{-10}	3.30×10^{-11}	7.97×10^{-11}	8.22×10^{-11}
	65%	6.06×10^{-11}	9.95×10^{-12}	2.98×10^{-11}	3.07×10^{-11}

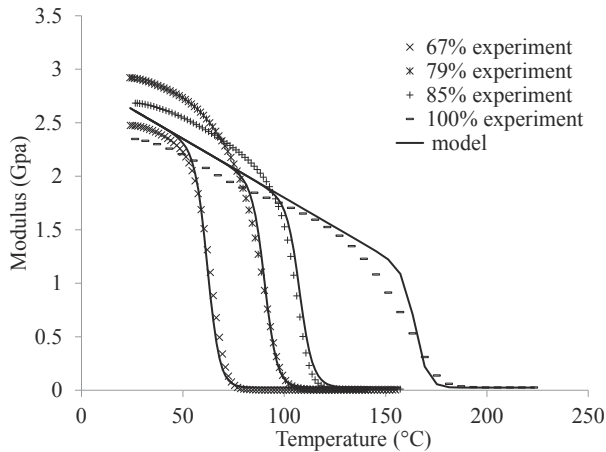


Fig. 9. Fitting of modulus experimental data for the XU3508 / XB3473 epoxy system.

$$a_r = a_{rub} + a_{rub}\alpha + \frac{(a_{glass} - a_{rub} - a_{rub}\alpha)}{1 + \exp(C_{TE}(T - T_g - \sigma_{CTE}))} \quad (31)$$

where a_{rub} , a_{glass} are the values of CTE for the uncured material in the rubber and glass state respectively and $a_{rub}\alpha$ the sensitivity of the rubber CTE on degree of cure. Fig. 10 illustrates the CTE experimental data and fitting. The average relative error of the fitting is 20%. The high average error is driven by the behaviour around glass transition at which the probe tends to depress the sample as it softens.

Fig. 11 shows the fitting of the shrinkage experimental data with the linear model of Eq. (27), corresponding to a relative error of 6%. Table 3 summarises the fitting parameters for the mechanical and thermo-mechanical constitutive models.

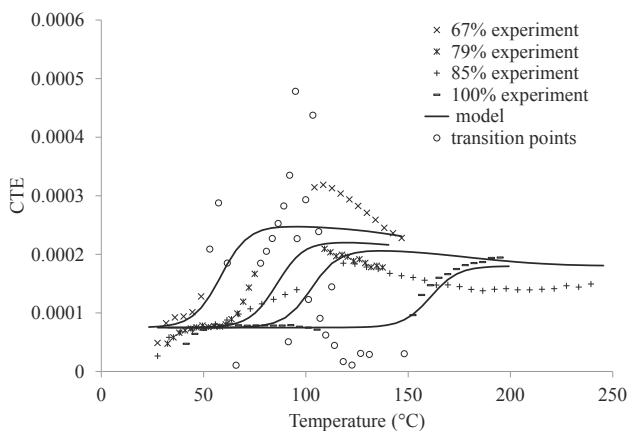


Fig. 10. Fitting of CTE experimental data for the XU3508 / XB3473 epoxy system.

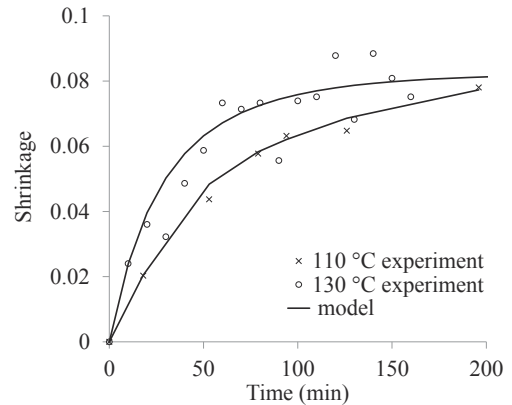


Fig. 11. Fitting of shrinkage experimental data for the XU3508 / XB3473 epoxy system.

5.3. Simulation results

5.3.1. Stage one

The results of the simulation at the exit of the pre-former die, which constitutes the end of stage one, are shown in Fig. 12. The computational time required for the stage one simulation is about 90 min on a standard desktop computer equipped with four processors. The final degree of cure at the end of stage one is 62%. The degree of cure evolution along the length of the profile is illustrated in Fig. 12a. A degree of cure in this region is appropriate to allow the material to complete stage one without running the risk to jam the pultrusion line due to low cure and to allow the bending in the post-former. Fig. 12b reports the degree of cure distribution through thickness at the exit of stage one. The distribution shows that the gradient through thickness is less than 2% and therefore negligible.

Fig. 13 illustrates the temperature, viscosity and degree of cure evolution at three different nodes, as specified in Fig. 2c as boundary, mid-thickness and noodle node. The minimum viscosity value reached is 15 mPa. The flow reaches a steady state condition within few millimetres from the entry point. The process parameters used allowed full impregnation of the reinforcement. No temperature overshoot occurs whilst gradients lower than 6 °C/mm can be observed through the thickness which guarantees a practically uniform degree of cure evolution. The results of the simulation have been validated by measuring the glass transition temperature of manufactured profiles at the exit of the pre-former using Modulated Differential Scanning Calorimetry (MDSC). The glass transition temperature has been measured at the centre and on the surface of the pultruded profile by cutting materials out of these regions and the results are reported in Fig. 14. The measured values are around 53 °C, corresponding to 65% degree of cure. The model prediction of 62% degree of cure at the exit of the pre-former is in good agreement with the measured values. The pre-cure level is close to the gelation point of the resin which according to the supplier [25] gels between 15 and 21 min at 160 °C. This corresponds to a degree of cure in the range of 63–73% as estimated using the cure kinetics of the resin system presented in Eq. (7).

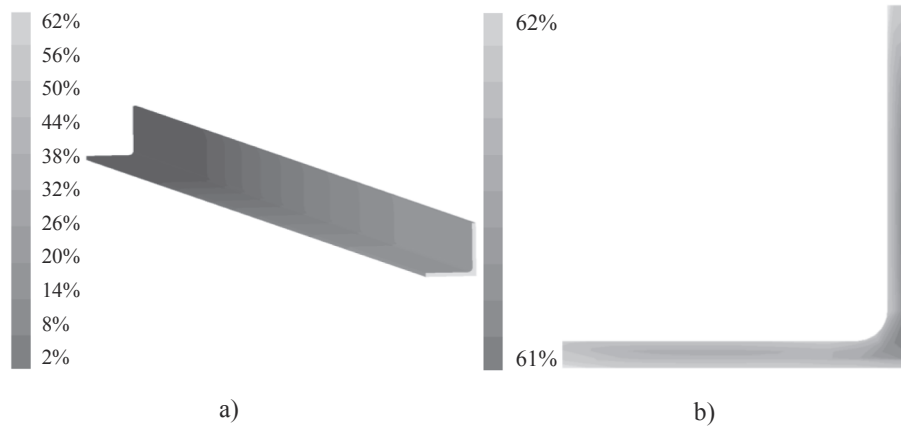


Fig. 12. Degree of cure distribution at the end of stage one a) along the pultrusion line; b) in the cross section.

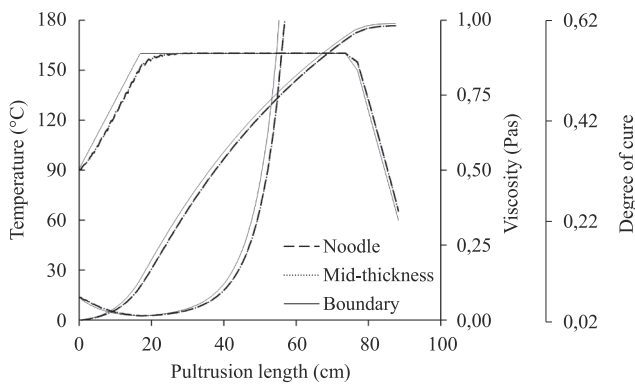


Fig. 13. Temperature, viscosity and degree of cure evolution along the pre-former during stage one at three different node locations defined in Fig. 2c.

5.3.2. Stage two

The outcome of stage one simulation in terms of degree of cure is set as the initial condition for stage two. Ambient temperature is set as the initial temperature since the material cools down between stage one and stage two. Since the degree of cure gradient through the thickness is negligible, a uniform initial degree of cure of 62% has been set. The 62% degree of cure at the stage one exit is a value close to gelation for the resin system under study. Therefore, the resin back flow at this point is assumed to be negligible. The low degree of cure facilitates the bending by allowing shear at entry of the die as the material is at significantly higher temperature than its glass transition. Interlayer shear is possible

for both UD and braid layers. The introduction of bending in the geometry results in curvature in the direction normal to the pre-existing curvature of the part from stage one. Consequently, the fillet regions involve a small double curvature governed by the large radius in the pultrusion direction. This can cause a small amount of shear, altering the nominal orientation of reinforcement fibres. At the pulling speed of 5 cm/min used, it takes about 20 min for a cross section of the stiffener to travel through the die, making the manufacture of one curved stiffener possible in 40 min. The overall duration of the simulation solution on a standard desktop computer equipped with four processors was about 20 h.

The three nodes illustrated in Fig. 2c (i.e. web node, noodle node and flange node) were used to examine the outcome of the simulation of stage two. Fig. 15a illustrates the temperature and degree of cure evolution for the cross sectional points as they travel within the die. The progression within the die is expressed as a function of angular position. The entry is at 0°. The temperature starts rising at -2° due to the proximity with the die entry. No temperature overshoot occurs during the process. The final degree of cure reached at the exit of the die is 87%. Fig. 15b shows the degree of cure distribution inside the post-former. A temperature drop occurs when the section goes past the last heater in the post-former which is located at about 51° and as a consequence the degree of cure settles at this point in time.

Fig. 16a illustrates the build-up of stress in the fibre direction in the post former for the 0° and 45° direction layers alongside temperature and the glass transition temperature development. Fig. 16b illustrates the build-up of stress in the transverse direction with respect to the fibres in the post former for the 0° and 45° direction layers. Fig. 15c shows the

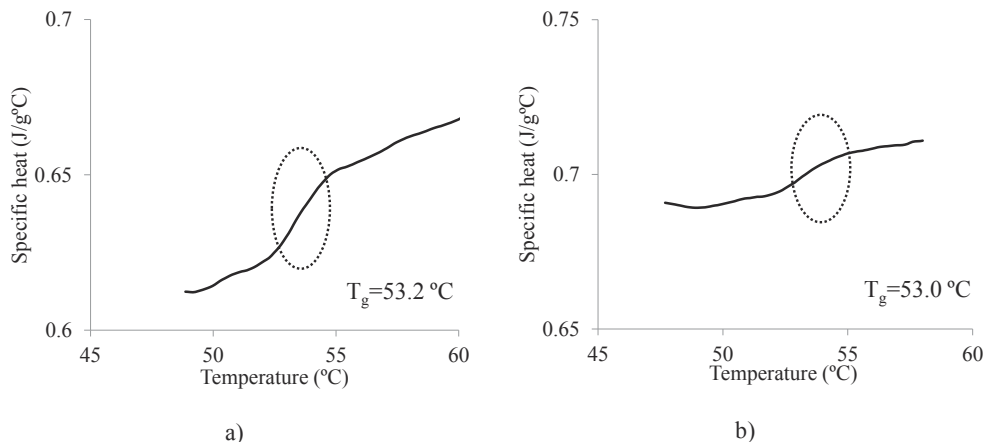


Fig. 14. Glass transition measurements of the pultruded profile at the end of stage one: a) on the surface; b) in the middle.

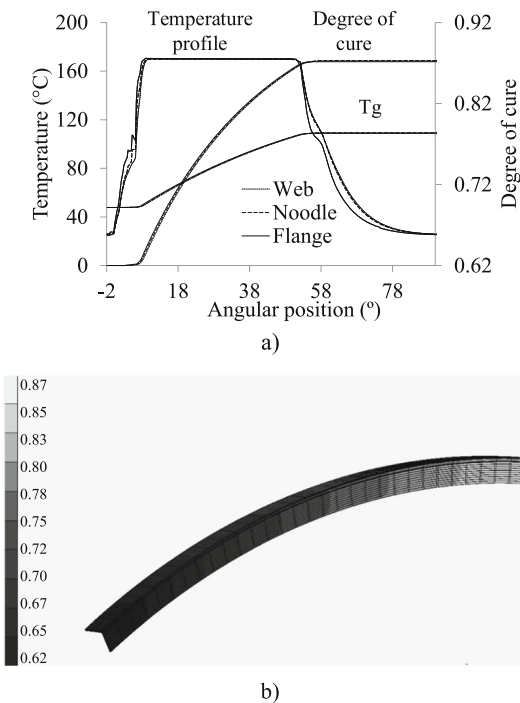


Fig. 15. a) Evolution of temperature and degree of cure for three nodes along the cross section; b) Degree of cure distribution along the profile length.

interlaminar stress for the 0° and 45° layers. The stress in the -45° direction is like the 45° direction. The node selected is located at the middle of the web and on the outer side. The node is depicted in Fig. 2c and denoted as 'External web'. The development of stress can be explained considering three phenomena: (i) bending due to contact with the die; (ii) thermal expansion/contraction and; (iii) cure shrinkage. The pulling force necessary to overcome contact forces in the curved die can be estimated by using the total reaction force at the nodes of the moving prescribed displacement boundary condition. The total force reaches a value of about 3.8 kN, once the material that entered the die at the beginning of the simulation reaches the exit, which corresponds to an average tensile stress of about 24 MPa. The levels of pulling force and associated tensile stress are sufficiently small to guarantee feasibility of the process. Fig. 17 illustrates the evolution of the pulling force which reaches steady state at about 20° within the post-former die. At the entry, the web comes in contact with the die creating a local tensile stresses which causes compressive stresses at locations radially opposite to it (Fig. 18a) and tensile stresses right before the entry. During heating up and before entering the die, the transverse-longitudinal expansion mismatch results in tensile stress in the fibre direction. After entering the die, the stress in the fibre direction is positive in the 45° layer and negative in the 0° layer due to the constraint with respect to expansion in the width direction imposed by the die. During the dwell, the stress generation is influenced by shrinkage; however, the material state changes from a degree of cure of about 67% at the beginning of the dwell to 87% at the end makes this effect relatively weak. At about 52°, the part begins to cool down. At this location the part is compressed in the fibre direction which results in generation of compressive stresses in 0° layers and tensile in 45° layers. At about 54°, the material in the flange vitrifies (Fig. 15a) causing compression in the fibre direction, whilst at the web location it has not vitrified yet. At 58°, there is a sharp change in stress. This is due to the fact that the material vitrifies at slightly different locations along the die for the different parts of the section (i.e. flange transition occurs earlier as it can be observed in Fig. 15a) with the part of the material reaching the glassy state constraining the expansion. Once the transition is completed in every location in the cross section, the transverse-longitudinal contraction

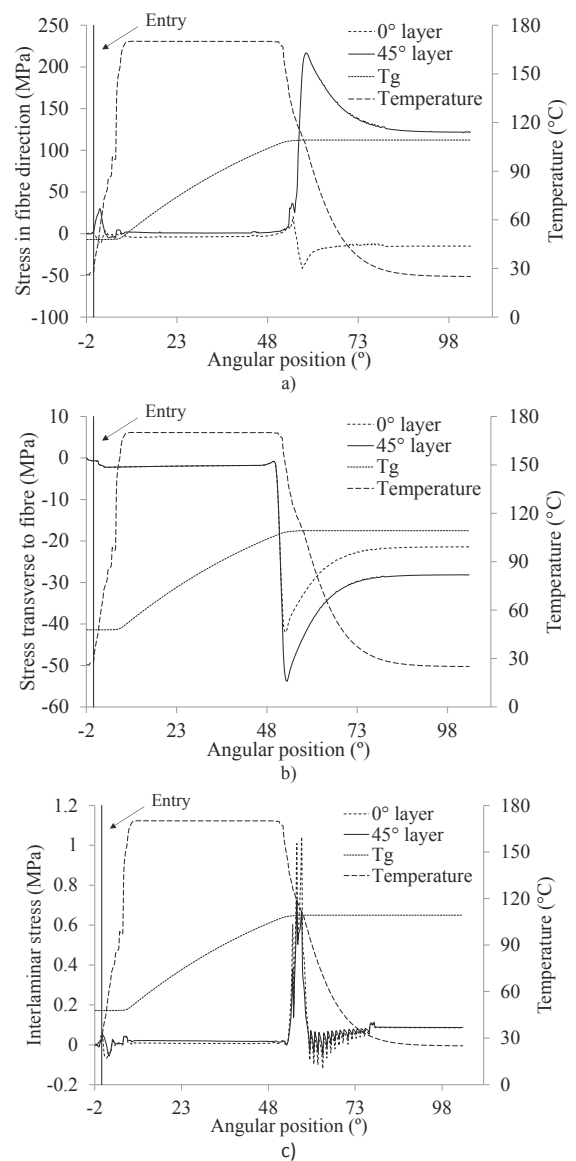


Fig. 16. Stress generated along the post-former at the 'External web' location: a) fibre direction; b) transverse to the fibre direction c) Interlaminar direction.

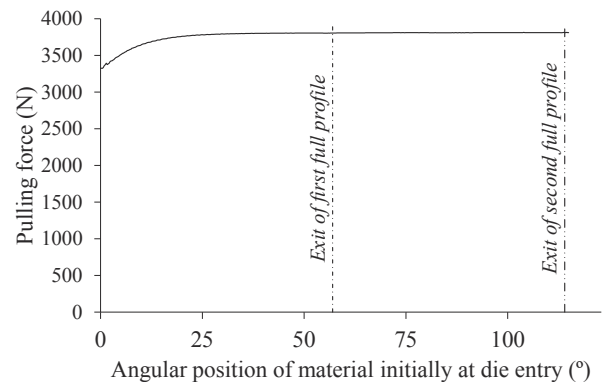


Fig. 17. Pulling force evolution during the process.

mismatch dominates resulting in a stress increases in the transverse to fibre direction and stress reduction in the fibre direction. This results in compression in 45° layers and tension in 0° layers due to the presence of

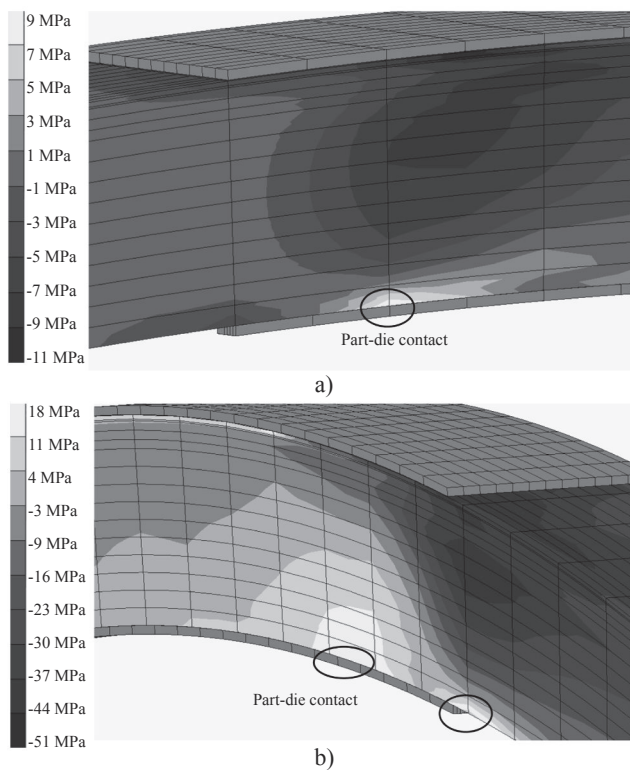


Fig. 18. Stress generated along the post-former due to part-die contact in fibre direction for the 0° layer: a) entry; b) exit.

the die which impedes the expansion in the transverse direction for 0° layers. At the exit, the part comes into contact with the die since the outside segment springs back when exiting causing local generation of tensile stresses (Fig. 18b) on the lower side. The interlaminar stress generated during the bending process (Fig. 16c) is very low (around 1 MPa). The oscillations after the exit are caused by repetitive contact with the die which are visible since the magnitude of interlaminar stress is lower than 1 MPa and the amplitude of the oscillation is about 0.2 MPa. The oscillation is the result of the alternation and opposing effect of pulling and spring back. The maximum level of compressive stress generated during the process is 54 MPa in the transverse direction of the 45° layers, whilst the maximum tensile stresses is 200 MPa, occurring in the fibre direction of 45° layers.

6. Conclusions

A pultrusion process concept able to produce curve components has been investigated using simulation. A material characterisation campaign has been undertaken to assess the rheological, mechanical and thermomechanical properties of the XU3508 epoxy / XB3473 hardener system leading to the formulation of phenomenological constitutive material models simulating the evolution of viscosity, modulus, CTE and shrinkage during the process. The material characterisation campaign provides results for the resin system used not present in literature. Furthermore, the phenomenological model built to describe CTE evolution constitute an attempt to express CTE behaviour with degree of cure evolution as an underlying variable. 3D simulation of the pultrusion has been carried out taking into account the flow through porous media, thermochemical and thermomechanical problems. The representation of thermochemical effects occurring during the phase in which flow through porous media also takes place are validated against experimental results from the pultrusion line. The simulation is able to predict the temperature and degree of cure at the exit of the pre-former and stress generated during the forming process in the post-former. The

simulation can be used to design optimal pre-curing conditions to allow the post-forming of the part. The assumption of uniform degree of cure holds for thin components, but in the case of thick components a procedure to pass the degree of cure at the end of stage one to the initial conditions of stage two needs to be implemented. Further extension of the model is to link it with an optimisation methodology to identify optimal cure cycles to minimise process time and cure induced defects. Additionally, the modular nature of the process allows manufacturing partially cured parts that can be used for secondary bonding such as co-curing (i.e. skin-stiffener).

Application to the curved stringer considered, showed that introducing the curvature is possible in the post-former when the part is pre-cured up to 62% in the pre-former. The bending in the post-former resulted in a maximum compressive stress of 54 MPa in the transverse direction and tensile stresses of 200 MPa in the fibre direction.

The results presented here demonstrated the feasibility of manufacturing aerospace quality parts using standard heated die pultrusion with the addition of a curved post-former based on a full 3D simulation of chemical-thermal-mechanical effects capable of predicting stresses within the manufactured part due to bending, cure and contact with the die. This highlights the potential of manufacturing of aerospace quality curved parts in a continuous process by introducing pre-former and post-former stages. Considering the significant cost benefits of pultrusion, the ability to introduce curvature can enhance efficiency and expand the application envelope of composites. In particular for curved aerospace components, continuous production can address the massive demand for these geometries in the context of single-aisle aircraft fuselage and the corresponding stringers, where metallic solution currently dominate the market.

CRedit authorship contribution statement

G. Struzziero: Conceptualization, Methodology, Investigation, Formal analysis, Writing - original draft. **G.M. Maistros:** Investigation, Validation. **J. Hartley:** Validation, Project administration, Funding acquisition. **A.A. Skordos:** Conceptualization, Funding acquisition, Writing - review & editing, Supervision.

Declaration of Competing Interest

The authors declare no conflict of interest.

Acknowledgements

This work was supported by the European Commission through the FP7 project PULAERO (Project ID: 605613). ESI group is kindly acknowledged for providing the license for PAMRTM®. Data underlying this study can be accessed through the Cranfield University repository at <https://doi.org/10.17862/cranfield.rd.13056638>.

References

- [1] Liu X-L. A finite element/nodal volume technique for flow simulation of injection pultrusion. *Compos A Appl Sci Manuf* 2003;34(7):649–61.
- [2] Liu XL. Iterative and transient numerical models for flow simulation of injection pultrusion. *Compos Struct* 2004;66(1):175–80.
- [3] Rahatekar SS, Roux JA. Numerical simulation of pressure variation and resin flow in injection pultrusion. *J Compos Mater* 2003;37(12):1067–82.
- [4] Rahatekar SS, Roux JA. Injection pultrusion simulation for polyester/glass mat/rovings/mat composites. *J Reinf Plast Compos* 2005;24(1):53–68.
- [5] Gadam SUK, Roux JA, McCarty TA, Vaughan JG. The impact of pultrusion processing parameters on resin pressure rise inside a tapered cylindrical die for glass-fibre/epoxy composites. *Compos Sci Technol* 2000;60(6):945–58.
- [6] Li S, Xu L, Ding Z, Lee LJ, Engelen H. Experimental and theoretical analysis of pulling force in pultrusion and resin injection pultrusion (rip) – part II: modeling and simulation. *J Compos Mater* 2003;37(3):195–216.
- [7] Yun MS, Lee WI. Analysis of pulling force during pultrusion process of phenolic foam composites. *Compos Sci Technol* 2008;68(1):140–6.
- [8] Simacek P, Advani SG. Simulating tape resin infiltration during thermoset pultrusion process. *Compos A Appl Sci Manuf* 2015;72:115–26.

- [9] Baran I, Tutum CC, Hattel JH, Akkerman R. Pultrusion of a vertical axis wind turbine blade part-I: 3D thermo-chemical process simulation. *Int J Mater Form* 2015;8(3):379–89.
- [10] Carlone P, Palazzo GS, Pasquino R. Pultrusion manufacturing process development by computational modelling and methods. *Math Comput Modell* 2006;44(7):701–9.
- [11] Chachad YR, Roux JA, Vaughan JG, Arafat ES. Thermal model for three-dimensional irregular shaped pultruded fiberglass composites. *J Compos Mater* 1996;30(6):692–721.
- [12] Joshi SC, Lam YC. Integrated approach for modelling cure and crystallization kinetics of different polymers in 3D pultrusion simulation. *J Mater Process Technol* 2006;174(1):178–82.
- [13] Lin Liu X, Crouch IG, Lam YC. Simulation of heat transfer and cure in pultrusion with a general-purpose finite element package. *Compos Sci Technol* 2000;60(6):857–64.
- [14] Liu XL. Numerical modeling on pultrusion of composite I beam. *Compos A Appl Sci Manuf* 2001;32(5):663–81.
- [15] Liu XL, Hillier W. Heat transfer and cure analysis for the pultrusion of a fiberglass-vinyl ester I beam. *Compos Struct* 1999;47(1):581–8.
- [16] Coelho RML, Calado VMA. An optimization procedure for the pultrusion process based on a finite element formulation. *Polym Compos* 2002;23(3):329–41.
- [17] Jianhua Li YCL, Joshi SC. Simultaneous optimization of die-heating and pull-speed in pultrusion of thermosetting composites. *Polym Compos* 2003;24(1):199–209.
- [18] Joshi SC, Lam YC, Win Tun U. Improved cure optimization in pultrusion with pre-heating and die-cooler temperature. *Compos A Appl Sci Manuf* 2003;34(12):1151–9.
- [19] Li J, Joshi SC, Lam YC. Curing optimization for pultruded composite sections. *Compos Sci Technol* 2002;62(3):457–67.
- [20] Acquah C, Datskov I, Mawardi A, Zhang F, Achenie LEK, Pitchumani R, et al. Optimization under uncertainty of a composite fabrication process using a deterministic one-stage approach. *Comput Chem Eng* 2006;30(6):947–60.
- [21] Santos LS, Pagano RL, Biscaia EC, Calado VMA. Optimum Heating Configuration of Pultrusion Process. In: de Brito Alves RM, do Nascimento CAO, Biscaia EC, editors. *Computer Aided Chemical Engineering*; Elsevier; 2009. p. 705–10.
- [22] Baran I, Akkerman R, Hattel JH. Modelling the pultrusion process of an industrial L-shaped composite profile. *Compos Struct* 2014;118:37–48.
- [23] Baran I, Tutum CC, Nielsen MW, Hattel JH. Process induced residual stresses and distortions in pultrusion. *Compos B Eng* 2013;51:148–61.
- [24] Britnell DJ, Tucker N, Smith GF, Wong SSF. Bent pultrusion—a method for the manufacture of pultrudate with controlled variation in curvature. *J Mater Process Technol* 2003;138(1):311–5.
- [25] Tena I, Sarrionandia M, Torre J, Aurrekoetxea J. The effect of process parameters on ultraviolet cured out of die bent pultrusion process. *Compos B Eng* 2016;89:9–17.
- [26] Edwards CM, D'hooghe EL. U.S. Patent No. 6,872,343. Washington, DC: US Patent and Trademark Office, 2005.
- [27] Jansen K, Weidler D, Hoffmann M. U.S. Patent No. 8,066,922. In: Washington DUSPaTO, editor, 2011.
- [28] TohoTenax, Delivery programme and characteristics Tenax HTA filament yarn, Toh Tenax Europe GMBH, 2011.
- [29] Huntsman® Resin XU 3508/ Hardeners XB 3403/ XB 3486/ Aradur® 22962/ Aradur® 2954/ Hardener XB 3473 Product data. www.huntsman.com; 2007.
- [30] Wurtz Release agents PAT®-656/B3R. www.epwuertz.de; 2003.
- [31] Struzziero G, Remy B, Skordos AA. Measurement of thermal conductivity of epoxy resins during cure. *J Appl Polym Sci* 2018;136(5):47015.
- [32] Khou L, Centea T, Hubert P. Characterization Methodology of Thermoset Resins for the Processing of Composite Materials — Case Study: CYCOM 890RTM Epoxy Resin. *J Compos Mater* 2010;44(11):1397–415.
- [33] Pascault JP, Williams RJJ. Relationships between glass transition temperature and conversion. *Polym Bull* 1990;24(1):115–21.
- [34] Skordos AA, Partridge IK. Inverse heat transfer for optimization and on-line thermal properties estimation in composites curing. *Inverse Prob Sci Eng* 2004;12(2):157–72.
- [35] Farmer JD, Covert EE. Thermal conductivity of a thermosetting advanced composite during its cure. *J Thermophys Heat Transfer* 1996;10(3):467–75.
- [36] Yamane T, Katayama S, Todoki M, Hatta I. The measurement of thermal conductivity of carbon fibers. *J Wide Bandgap Mater* 2000;7(4):294–305.
- [37] Vaughan TJ, McCarthy CT. Micromechanical modelling of the transverse damage behaviour in fibre reinforced composites. *Compos Sci Technol* 2011;71(3):388–96.
- [38] Zimmermann K, Van Den Broucke B. Assessment of process-induced deformations and stresses in ultra thick laminates using isoparametric 3D elements. *J Reinf Plast Compos* 2012;31(3):163–78.
- [39] Schapery RA. Thermal expansion coefficients of composite materials based on energy principles. *J Compos Mater* 1968;2(3):380–404.
- [40] Pradere C, Sauder C. Transverse and longitudinal coefficient of thermal expansion of carbon fibers at high temperatures (300–2500K). *Carbon* 2008;46(14):1874–84.
- [41] Li C, Potter K, Wisnom MR, Stringer G. In-situ measurement of chemical shrinkage of MY750 epoxy resin by a novel gravimetric method. *Compos Sci Technol* 2004;64(1):55–64.
- [42] PAMRTM®, ESI Group 2013 www.esi-group.com.
- [43] Marc® volume A: Theory and user information. www.mscsoftware.com, 2015.
- [44] Marc® volume B: Element library. www.mscsoftware.com, 2015.
- [45] Marc® volume D: User subroutines and special routines. www.mscsoftware.com, 2015.
- [46] Antonucci V, Giordano M, Inserraimparato S, Nicolais L. Analysis of heat transfer in autoclave technology. *Polym Compos* 2001;22(5):613–20.
- [47] Struzziero G, Skordos AA. Multi-objective optimisation of the cure of thick components. *Compos A Appl Sci Manuf* 2017;93:126–36.
- [48] Mesogitis TS, Skordos AA, Long AC. Stochastic heat transfer simulation of the cure of advanced composites. *J Compos Mater* 2015;50(21):2971–86.
- [49] Shanku R, Vaughan JG, Roux JA. Rheological characteristics and cure kinetics of EPON 862/W epoxy used in pultrusion. *Adv Polym Tech* 1997;16(4):297–311.
- [50] Hoagland D, George A. Continuous permeability measurement during unidirectional vacuum infusion processing. *J Reinf Plast Compos* 2017;36(22):1618–28.
- [51] Long AC. Process modelling for liquid moulding of braided preforms. *Compos A Appl Sci Manuf* 2001;32(7):941–53.
- [52] Gebart BR. Permeability of Unidirectional Reinforcements for RTM. *J Compos Mater* 1992;26(8):1100–33.

Materials modelling and process simulation of the pultrusion of curved parts

Struzziero, Giacomo

2021-02-11

Attribution 4.0 International

Struzziero G, Maistros GM, Hartley J, Skordos AA. (2021) Materials modelling and process simulation of the pultrusion of curved parts. *Composites Part A: Applied Science and Manufacturing*, Volume 144, May 2021, Article number 106328

<https://doi.org/10.1016/j.compositesa.2021.106328>

Downloaded from CERES Research Repository, Cranfield University